Environmental Science & Technology

Article

pubs.acs.org/est

Biotic and Abiotic Interactions in Aquatic Microcosms Determine Fate and Toxicity of Ag Nanoparticles. Part 1. Aggregation and Dissolution

Jason M. Unrine,*[,†,#,¶] Benjamin P. Colman,[‡,#,¶] Audrey J. Bone,[§,#] Andreas P. Gondikas,[∥,#] and Cole W. Matson[⊥,#]

[†]Department of Plant and Soil Sciences, University of Kentucky, Lexington, Kentucky 40546, United States

[‡]Biology, Duke University, Durham, North Carolina 27708, United States

[§]Nicholas School of the Environment, Duke University, Durham, North Carolina 27708, United States

[∥]Pratt School of Engineering, Duke University, Durham, North Carolina 27708, United States

[⊥]Department of Environmental Science, Baylor University, Waco, Texas 76798, United States

[#]Center for the Environmental Implications of NanoTechnology, Duke University, Durham, North Carolina 27708, United States

Supporting Information

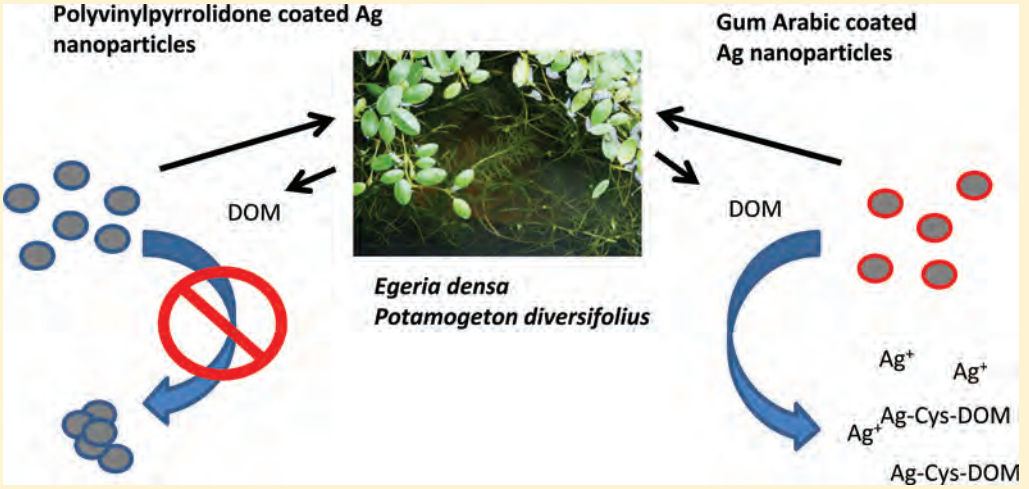

ABSTRACT: To better understand their fate and toxicity in aquatic environments, we compared the aggregation and dissolution behavior of gum arabic (GA) and polyvinylpyrrolidone (PVP) coated Ag nanoparticles (NPs) in aquatic microcosms. There were four microcosm types: surface water; water and sediment; water and aquatic plants; or water, sediment, and aquatic plants. Dissolution and aggregation behavior of AgNPs were examined using ultracentrifugation, ultrafiltration, and asymmetrical flow field flow fractionation coupled to ultraviolet−visible spectroscopy, dynamic and static laser light scattering, and inductively coupled plasma mass spectrometry. Plants released dissolved organic matter (DOM) into the water column either through active or passive processes in response to Ag exposure. This organic matter fraction readily bound Ag ions. The plant-derived DOM had the effect of stabilizing PVP-AgNPs as primary particles, but caused GA-AgNPs to be removed from the water column, likely by dissolution and binding of released Ag ions on sediment and plant surfaces. The destabilization of the GA-AgNPs also corresponded with X-ray absorption near edge spectroscopy results which suggest that 22−28% of the particulate Ag was associated with thiols and 5−14% was present as oxides. The results highlight the potential complexities of nanomaterial behavior in response to biotic and abiotic modifications in ecosystems, and may help to explain differences in toxicity of Ag observed in realistic exposure media compared to simplified laboratory exposures.

INTRODUCTION

In recent years, there has been considerable interest in toxicity testing for manufactured Ag nanoparticles (AgNPs) due to the proliferation of their use in consumer and medical products such as polymers, textiles, cosmetics, and other primarily antimicrobial applications.[1] However, toxicity studies often lack

Special Issue: Transformations of Nanoparticles in the Environment

Received: December 27, 2011
Revised: March 26, 2012
Accepted: March 27, 2012
Published: March 27, 2012

dx.doi.org/10.1021/es204682q | Environ. Sci. Technol. 2012, 46, 6915−6924

characterization of the aggregation and dissolution behavior of AgNPs in toxicity testing media and such media are often simplified relative to real world exposures.[2] Aggregation and dissolution of AgNPs can both be modified by environmental factors such as solution pH, ionic strength, dissolved oxygen, and natural organic matter content,[2−6] and these modifications can also result in altered bioavailability and toxicity of AgNPs. Despite this, the vast majority of toxicity studies of AgNPs have been conducted in simplified aquatic toxicity or tissue culture testing media containing only inorganic salts.[7] We expect that AgNPs in natural ecosystems will be subject to interactions with abiotic and biotic ecosystem components, and that these interactions will likely be dynamic (e.g., plant exudates may modify the behavior of colloidal particles by changing their surface chemistry in addition to their effects on metal bioavailability[10]).

To help elucidate interactions between abiotic and biotic ecosystem components that influence AgNP behavior, we established aquatic microcosms containing an array of environmental matrices: water (W); water and sediment (WS); water and aquatic plants (WP); or water, aquatic plants, and sediment (WPS). The objective of this study was to describe the resulting aggregation and dissolution behavior of AgNPs in the water compartment of these microcosms, and to investigate the role of sediment and aquatic plants on particle stability. This is the first of a pair of papers; the second paper describes the influence of these biotic and abiotic components on Ag speciation and toxicity in zebrafish and *Daphnia*.[8]

To accomplish our objectives, we used asymmetrical flow field flow fractionation (AF4) separations with multidetection in combination with batch filtration techniques to uncover the influence of microcosm components on AgNP aggregation and dissolution behavior. Separations of AgNPs based on field flow fractionation (FFF) have recently been reported for both symmetrical flow field flow fractionation (SF4)[9] and sedimentation field flow fractionation (SedFFF).[10] Because flow-based FFF techniques lack a stationary phase, to which NPs may irreversibly bind,[11] and are selective in the range of ∼2−800 nm, it is ideal for separating primary nanoparticles from aggregates. Sedimentation FFF techniques also lack a stationary phase, and have excellent resolution for dense particles such as Ag, but they can only resolve Ag particles larger than about 20 nm and the density of aggregates must be known to determine their size.[13] The use of light scattering, ultraviolet−visible (UV−vis) and inductively coupled plasma mass spectrometer (ICP-MS) detectors provides information on particle size, aggregation state, and elemental composition, respectively.[12]

EXPERIMENTAL SECTION

Microcosm Setup. Details of microcosm design and dosing are available in Bone et al.[8] In brief, microcosms were established for four different environmental matrices: water only (W), water+sediment (WS), water+plants (WP), and water+plants+sediments (WPS). All microcosms contained 600 mL of water. Matrices including sediment contained 200 g of sediment, and matrices with plants contained 3 g of *Potamogeton diversifolius* and 6 g of *Egeria densa*. The microcosm plant biomass (286 g wet mass m^{-2}) is similar to what has been reported in lotic habitats in the southeastern United States.[13] Four treatments were prepared in triplicate for each matrix: control, $AgNO_3$, GA-AgNP, and PVP-AgNP. Silver treatments were applied at 2.0 mg L^{-1} Ag. Control, GA-AgNP, and PVP-AgNP received 0.32 mg/L KNO_3 to control for the addition of NO_3^- with the $AgNO_3$. Microcosms were incubated for 24 h at 25 °C on an 18 h light:6 h dark light cycle under cool fluorescent lamps. At 24 h, water samples were decanted from the microcosms for acute toxicity testing, water quality, and Ag characterization and quantification. Samples for AF4 analysis were stored at 4 °C in the dark.

Particle Synthesis and Characterization. The synthesis, purification, and basic characterization of the particles have been described previously.[14] We performed additional particle size characterization using transmission electron microscopy (TEM) and analyzed electrophoretic mobility using phase analysis light scattering (PALS). The particles were also characterized with respect to oxidation state using X-ray absorption near edge spectroscopy (XANES).[8] Hydrodynamic radius was obtained using AF4-ICP-MS (*vide infra*).

ICP-MS Analysis of Bulk and Fractionated Samples. For total Ag analysis, water samples were analyzed whole, filtered to 0.7 μm using ashed binder-free borosilicate filters, and filtered using 3 kDa molecular weight cutoff (MWCO) regenerated cellulose ultracentrifugation devices to assess the total, colloidal, and dissolved Ag concentrations, respectively. Recovery of stock AgNPs through the 0.7-μm filters was >90%. Recovery of Ag ions through the 3 kDa filters is typically 75−85%. Because the 3 kDa ultrafiltration devices could remove some Ag ions bound to larger DOM, we also analyzed supernatants from ultracentrifuged samples (ultrasupernatants). Samples were centrifuged at 239 311*g* for either 90 min (PVP, $AgNO_3$) or 115 min (GA) in order to remove Ag particles larger than 4 and 1 nm, respectively. A longer centrifugation time was used for GA-AgNPs because some particles may have been present with diameters <4 nm. These same parameters would only remove material of the density of DOM (1.5 g/mL) estimated to be larger than 7−10 nm, so the difference in centrifugation times would not have affected concentrations of dissolved, complexed, or DOM-bound constituents, which would not have been removed by either centrifugation program. All samples were acidified to dissolve AgNPs (AgCl and Ag_2S may not have been completely dissolved) and preserve them by bringing them to 0.15 M HNO_3 before analysis by ICP-MS (Agilent 7500cx or Agilent 7700cx, Santa Clara, CA, USA). We included blanks and standard reference materials (SRM 1643e, Trace Elements in Water, National Institute of Standards and Technology, Gaithersburg, MD, USA) as quality control samples. The method detection limit (MDL) was 0.009 μg L^{-1}. Recovery of the standard reference material averaged 88.2 ± 0.4% (mean ± standard deviation; n = 6). For statistical comparisons we performed ANOVA with Tukey's multiple comparisons (SAS version 9.2, Cary, NC, USA). Normality was tested using the Shapiro−Wilk test and homogeneity of variance was tested using the Bartlett test. The unfiltered Ag concentrations had to be log transformed to homogenize variance among treatments. We substituted 1/2 of the MDL for observations below the MDL for statistical purposes.

AF4 Multidetection Analysis. We filtered the microcosm water samples using 30-mm, 1.0-μm pore size, borosilicate glass fiber syringe filters (GE Osmonics, Fairfield, CT, USA). Asymmetrical flow field flow fractionation separations were performed using a Wyatt Technologies, Eclipse 3 (Santa Barbara, CA, USA). A description of the AF4 running conditions is provided in Table S1. The AF4 eluent was directed to a UV−vis diode array detector (Agilent 1200

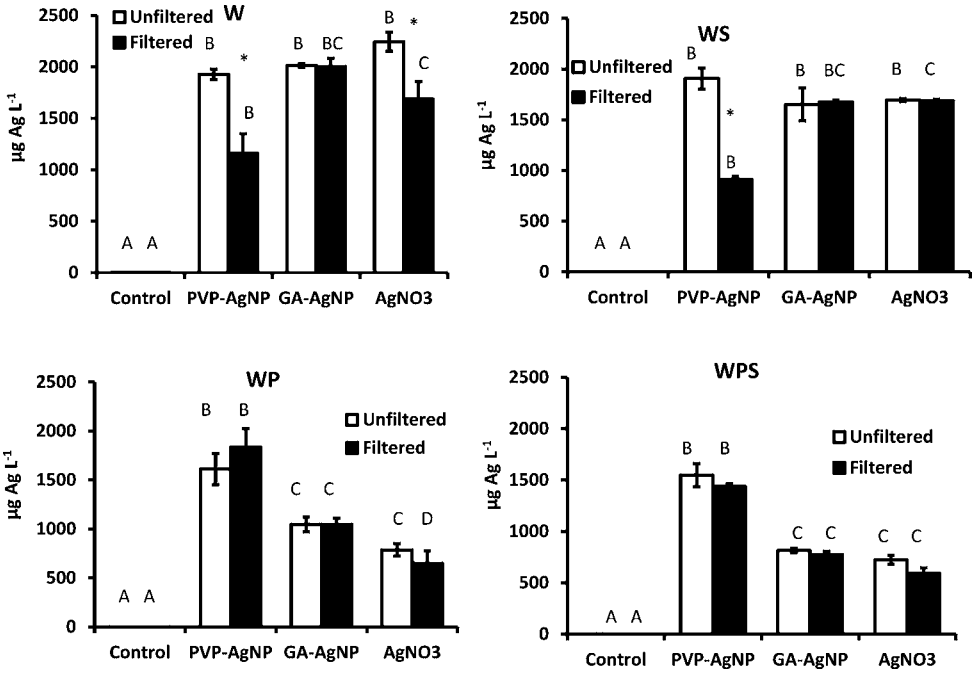

Figure 1. Ag concentrations in filtered (0.7 μm) versus unfiltered water samples for control, polyvinylpyrrolidone-coated Ag nanoparticles (PVP-AgNP), gum Arabic-coated Ag nanoparticles (GA-AgNP), and $AgNO_3$-treated microcosms containing water (W), water and sediment (WS), water and plants (WP), or water, plants, and sediment (WPS). Bars with the same letter are not significantly different ($p < 0.05$) among treatments (control, PVP-AgNP, GA-AgNP, $AgNO_3$) for the same sample type (unfiltered or filtered) and matrix. Bars may have more than one letter; if any letter is the same as any letter over another bar, the two are not significantly different. An asterisk (*) indicates that filtered and unfiltered are significantly different ($p < 0.05$).

series), an 18-angle light scattering detector which was also equipped with a dynamic light scattering (DLS) detector at 100.3°, and finally directed to an ICP-MS (Agilent 7500cx; Santa Clara, CA, USA). The operating parameters for the ICP-MS are listed in Table S2. The DAD fractograms were collected at 420 nm for PVP-AgNP and 400 nm for the GA-AgNPs. Full spectra were also collected over the range of 300−500 nm to assess shifts in the surface plasmon resonance absorption band. The data from the DAD were collected and analyzed using Agilent Chemstation software, light scattering data were analyzed using Wyatt ASTRA software, version 5.3.4.11, and ICP-MS fractograms were processed using Agilent ICP-MS chromatographic software version C.01.00. To determine recovery of material from the channel, we injected particles with minimal (0.03 mL min^{-1}) cross-flow and compared the obtained area from these injections to the total areas of the chromatograms using the ICP-MS. The areas used to calculate recovery included the void and washout peaks, accounting for all particles leaving the channel. Samples from control mesocosms were analyzed as blanks to assess carryover of Ag in the fractograms.

Validation of AF4-Separations. We validated AF4 size separation by analyzing NIST traceable polystyrene latex spheres (20, 47, and 200 nm diameters, Thermo Scientific) and standard reference Au nanoparticles (30 and 60 nm nominal diameters, NIST SRMs 8012 and 8013, respectively). The 60 nm Au spheres were used to estimate channel thickness (necessary for correction due to swelling of the ultrafiltration membrane) using AF4 theory.[15] Sizes for particles displayed in the fractograms were calculated using Wyatt Chromatogram version 1.04 based on retention times AF4 theory. These retention times were cross validated by comparing to calibration curves of retention time versus diameter of the reference particles. Finally, the calibrated values were compared to values obtained using dynamic (DLS) and multiangle laser light scattering (MALLS).

RESULTS AND DISCUSSION

TEM and PALS Analysis. The PVP-AgNPs had a mean geometric primary particle (TEM) diameter of 49.3 ± 22.5 (mean ± standard deviation) and ranged from 5.0 to 113.9 nm in size; the GA-AgNPs had a mean geometric primary particle diameter of 12 ± 9.2 nm and ranged in size from 1.7 to 57.3 nm. Full details are presented in the Supporting Information (Figure S1). Zeta potential data in DI water (pH 5.8), 50%, and 100% synthetic moderately hard reconstituted water (MHW; pH 6.8) are presented in Table S3. The GA-AgNPs were negatively charged in all three matrices, while the PVP-AgNPs had a negative charge in DI water, but a nearly neutral to slightly positive charge in 50 and 100% MHW. This indicates that while electrostatic stabilization was likely important for GA-AgNPs, steric stabilization mechanisms may have been more important for PVP-AgNPs.

Batch Filtration and Ultracentrifugation. The batch 0.7 um filtration analyses suggested that extensive aggregation only occurred in the PVP-AgNP treated W and WS matrices. Analyses of unfiltered samples indicated significant losses of Ag from the water column when sediment or plants were present, particularly for the $AgNO_3$ and GA-AgNP treatments. There were significant differences in total Ag concentrations among treatments in unfiltered samples ($F_{15,32} = 1628$, $p < 0.001$; Figure 1). The total Ag concentrations in the unfiltered samples were similar to nominal concentrations in the W matrices for all treatments, indicating minimal losses to container walls. In the WS matrix, Ag concentrations for the GA-AgNP and $AgNO_3$ treatments were approximately 25% lower than the nominal

dx.doi.org/10.1021/es204682q | Environ. Sci. Technol. 2012, 46, 6915−6924

concentration of 2000 μg Ag L^{-1} in the W matrix. In the WP and WPS treatments, the unfiltered concentrations were also approximately 25% lower than nominal for PVP-AgNP, but the GA-AgNP and $AgNO_3$ treatments had concentrations that were approximately 50−75% lower than the nominal concentrations. There were also significant treatment dependent differences in total Ag concentrations in the filtered samples ($F_{15,32}$ = 316.29, p < 0.001). The concentrations in the unfiltered samples were similar to those in the 0.7-μm filtered samples for most treatment matrix combinations with the only large differences occurring with PVP-AgNPs in the W and WS matrices, and the GA-AgNPs in the WPS matrix (p < 0.05; Figure 1). For the PVP-AgNP samples, the 0.7-μm filtered samples had concentrations that were approximately 30−50% lower than concentrations observed in the unfiltered samples. Concentrations in the $AgNO_3$ treatment were slightly lower in the 0.7-μm filtered samples than the unfiltered samples in all matrices except WS. These results suggest that aggregation in the water column (hetero- or homoaggregation) resulting in the formation of aggregates >0.7 μm in diameter was occurring in the W and WS matrices for the PVP-AgNPs. This pattern was not observed for the GA-AgNPs, where the 0.7-μm filtrates had concentrations similar to the unfiltered samples.

Comparison of ultrafiltrate and ultrasupernatant concentrations indicated that a significant proportion of procedurally defined dissolved Ag was actually bound to material >3 kDa (equivalent to 0.9 nm) in matrices containing plants. This effect was most pronounced for the $AgNO_3$ and GA-AgNP treatments. Ag concentrations in the ultrafiltrates were in the low μg L^{-1} range for PVP-AgNPs except for the WPS matrix (Figure 2) and significant matrix dependent differences were observed ($F_{15,31}$ = 28.47, p < 0.001). The ultrafiltrate Ag concentrations for the GA-AgNP treatments were similar to the $AgNO_3$ ultrafiltrate concentrations in all matrices except for WPS, where $AgNO_3$ had approximately twice the ultrafiltrate Ag concentration of GA-AgNPs. Significant treatment-dependent differences were observed for the ultrasupernatants (Figure 3; $F_{14,33}$ = 24.31, p < 0.001) as well. In the majority of samples, ultrafiltrate concentrations were lower than the ultrasupernatant concentrations for all treatment combinations (Figure 2). The same trends of differences in concentrations for a given microcosm matrix among treatments was observed for both ultrafiltrate and ultrasupernatant. An exception to this trend was in the WS microcosms, where ultrafiltrate concentrations for GA-AgNPs were similar to those for $AgNO_3$, while in the ultrasupernatant the concentration in GA-AgNPs was much lower than that in $AgNO_3$. This suggests that there was a larger proportion of Ag bound to DOM in the PVP-AgNP and $AgNO_3$ treatments than for the GA-AgNP treatment in the WS matrix, since the difference in concentrations between ultrafiltrate and ultrasupernatant was much greater for PVP-AgNP and $AgNO_3$ treatments than for the GA-AgNP treatment . A large portion of the ultrasupernatant fraction was likely bound to DOM since the ultrafiltrate concentrations are much lower than the ultrasupernatant concentrations. Some DOM could have remained within the retentate of the ultrafiltration, but would not have been removed by ultracentrifugation. Humic and fulvic substances from aquatic sources can be >3 kDa, but smaller than the >7−10 nm cutoff that would have been removed by ultracentrifugation.[16] Larger organic matter from plant material would have also been retained. Supporting evidence is discussed in the next section on AF4 analysis to demonstrate that the organic matter present in the WP and

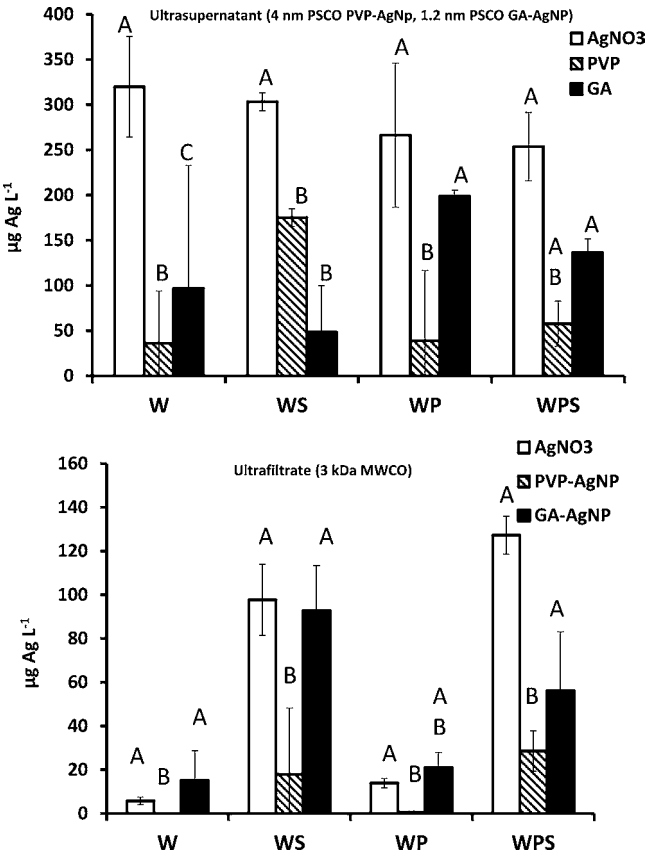

Figure 2. Ag concentrations in water samples that were ultrafiltered with a 3-kDa molecular weight cutoff (MWCO) filter, or ultracentrifuged to either a 4-nm Ag particle size cutoff (PSCO) for control and polyvinylpyrrolidone-coated Ag nanoparticles (PVP-AgNP), or 1 nm for gum Arabic-coated Ag nanoparticles (GA-AgNP)-, and $AgNO_3$ treated microcosms containing water (W), water and sediment (WS), water and plants (WP), or water, plants, and sediment (WPS). Bars within the same letter are not significantly different within the same microcosm type (p < 0.05).

WPS treatments is >3 kDa. The PVP and GA polymers would not have permeated the filter, having molar masses of 55 kDa and around 600 kDa, respectively.[17] It is also important to note that $AgCl_2$ formed in the $AgNO_3$ treatment[8] could have been removed by both ultrafiltration and ultracentrifugation.

AF4-Multidetector Analysis. Clear differences in the particle size distribution for PVP-AgNPs were observed between matrices that contained plants and those that did not (Figure 3). In the matrices with plants (WP and WPS), relatively narrow (full width at half-maximum [fwhm] = 6 min) symmetrical peaks were observed at retention times (t_r ~10.5 min) which were slightly smaller than those for the injected PVP-AgNP standards (t_r ~ 11.5 min) for the ICP-MS detector. Very broad peaks were observed for matrices without plants (W and WS; t_r = 17 min, fwhm = 12 min). The mean diameter for primary particles based on the ICP-MS retention estimated from calibration to reference particles was 62 nm, while the mean diameter of the aggregates was about 130 nm. The presence of intact primary particles was confirmed in peaks for all treatments by examining the surface plasmon resonance absorption bands recorded by the DAD detector (Figure 4). The spectra had a peak wavelength of 420 nm for the primary particle standards, as well as for the W, WP, and WPS treatments. The surface plasmon was shifted to 427 nm in the

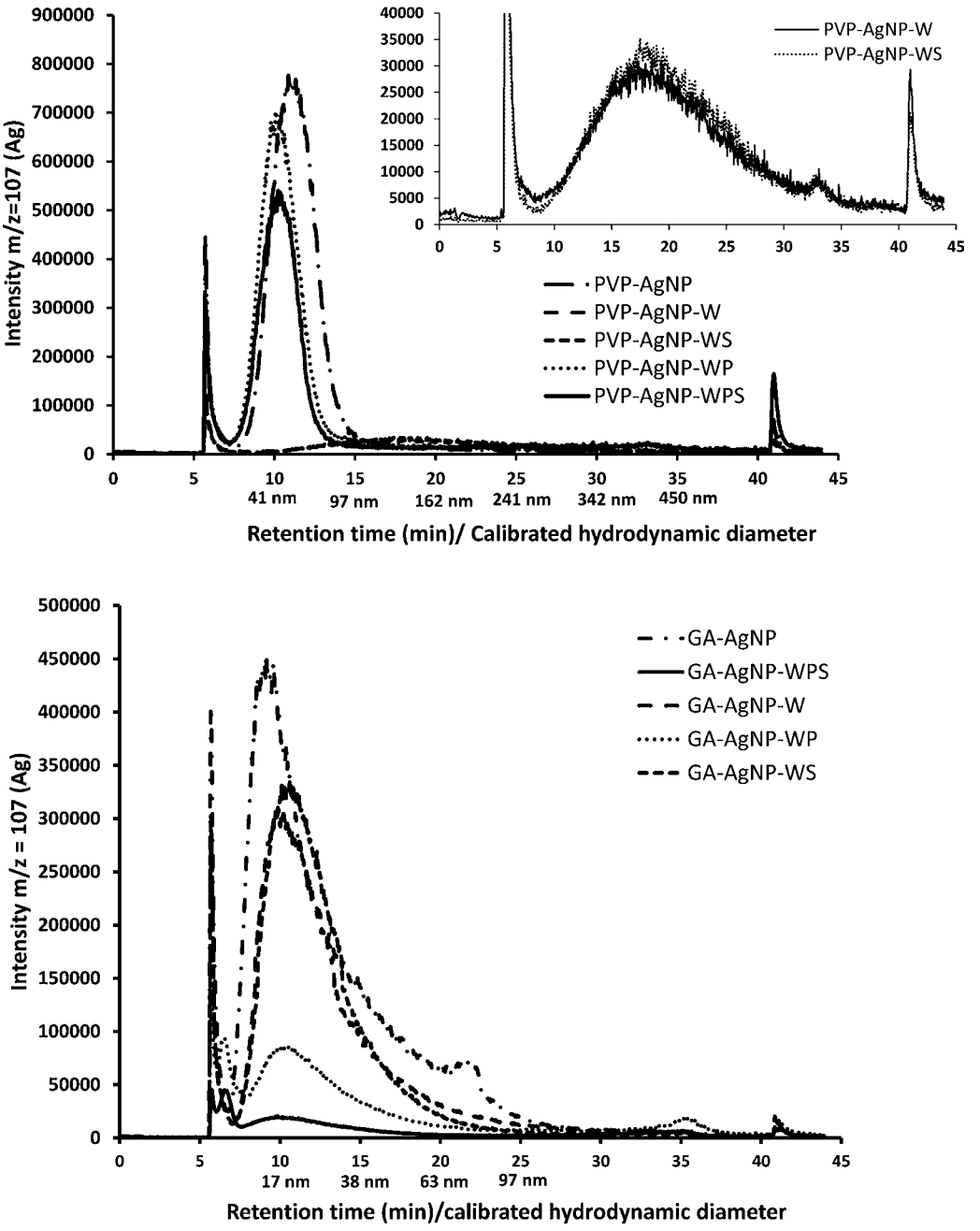

Figure 3. Asymmetrical flow field flow fractograms for control, polyvinylpyrrolidone-coated Ag nanoparticles (PVP-AgNP), gum Arabic-coated Ag nanoparticles (GA-AgNP), and $AgNO_3$ treated microcosms containing water (W), water and sediment (WS), water and plants (WP), or water, plants, and sediment (WPS). Calibrated hydrodynamic diameters are shown below the retention times on the *x* axes. The traces labeled PVP-AgNP and GA-AgNP are for PVP-AgNP and GA-AgNP standards. The starting cross-flow for the PVP-AgNP fractograms was 0.3 mL min^{-1} decreasing to 0.03 mL min^{-1} in 30 min. The starting cross-flow for the GA-AgNP fractograms was 1.0 mL min^{-1} decreasing to 0.03 mL min^{-1} in 30 min. The retention time for the void peak is 5.7 min.

WS treatment. When homoaggregation dominates, the surface plasmon absorption wavelength is red-shifted as interparticle distances become smaller than the particle dimensions.[17] When the concentration of Ag nanoparticles within an aggregate is low, such as in a homoaggregate, interparticle distances are expected to be greater than particle dimensions and a redshift in the surface plasmon absorption band is not expected to occur (Figure S2). The combination of size and surface plasmon absorption peak confirms the presence of primary particles for the WP and WPS treatments. Because the particle sizes were larger for the W treatment, but there was no shift in the surface plasmon peak, it is likely that PVP-Ag NPs were present in heteroaggregates. The WS treatment may have contained some homoaggregates, however the shift in the surface plasmon resonance band was too small to be definitive. The particle size distributions for aggregates in the W and WS treatments were very similar, suggesting that similar heteroaggregation processes dominated in these two matrices. These observations may be reflective of what is expected at trace-concentrations in the environment, since there were few direct AgNP−AgNP interactions, which could occur at higher concentrations.

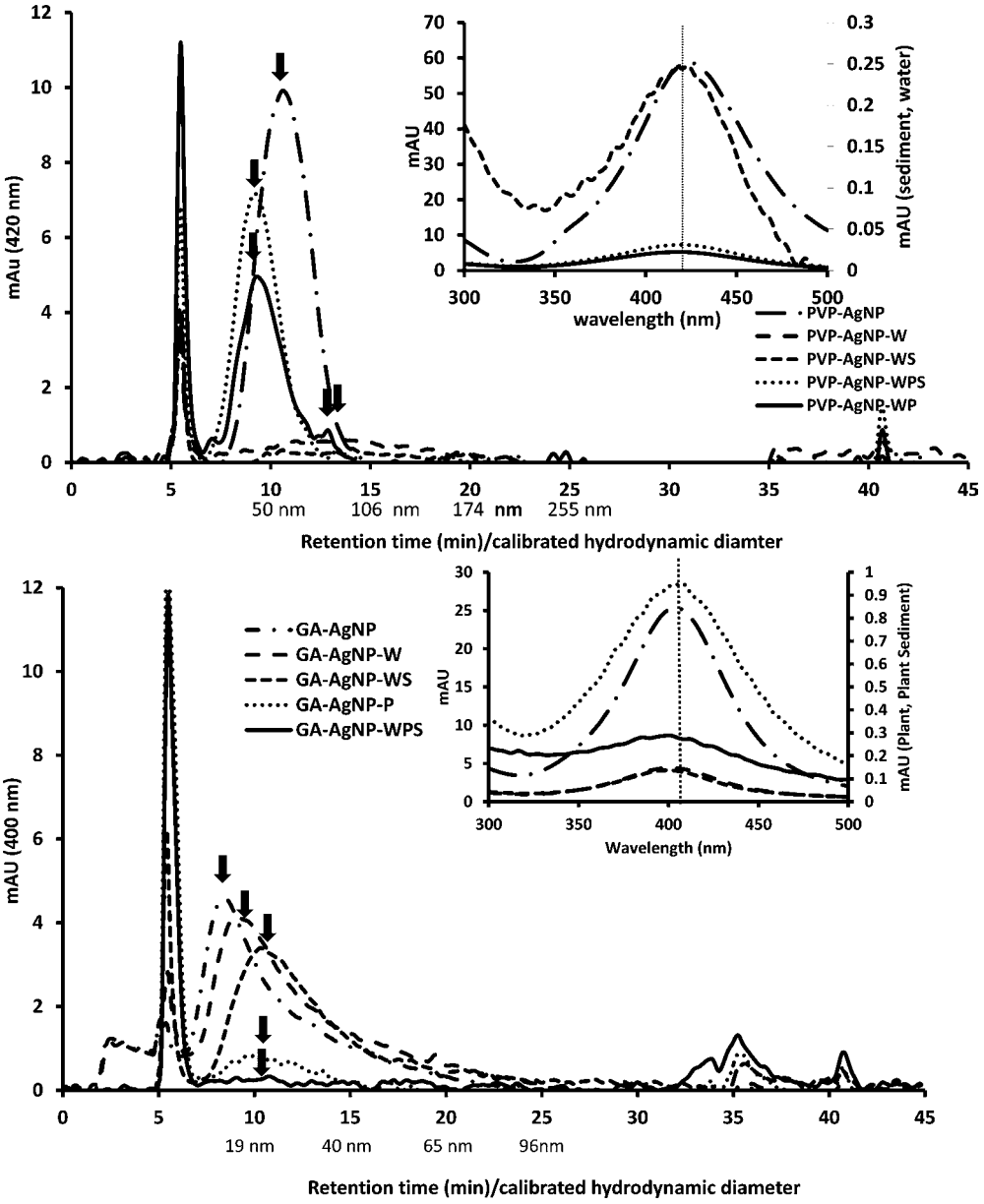

Figure 4. Asymmetrical flow field flow fractograms using ultraviolet−visible (UV−vis) diode array detection for polyvinylpyrrolidone-coated Ag nanoparticles (PVP-AgNP), gum Arabic-coated Ag nanoparticles (GA-AgNP), and $AgNO_3$ treated microcosms containing water (W), water and sediment (WS), water and plants (WP), or water, plants, and sediment (WPS). Calibrated hydrodynamic diameters are shown below the retention times on the *X* axes. The traces labeled PVP-AgNP and GA-AgNP are for PVP-AgNP and GA-AgNP standards. The starting cross-flow for PVP-AgNPs was 0.3 mL min^{-1} decreasing to 0.03 mL min^{-1} in 30 min. The starting cross-flow for GA-AgNPs was 1.0 mL min^{-1} decreasing to 0.03 mL min^{-1} in 30 min. The retention time for the void peak is 5.5 min.

The GA-AgNPs behaved very differently than PVP-AgNPs in response to the different matrices. Particle concentrations were reduced in the presence of plants and sediment, but little aggregation was observed. There were slight shifts in the ICP-MS peak retention times based on matrix, but in general these increased retention times were less than 2 min (Figure 3). Also, the overall shape of the ICP-MS fractograms was similar among treatments except that an additional peak appeared between the void peak and the primary particle peak at 5.8 min that may have corresponded to DOM-bound Ag. The quantity of Ag present within the fractograms was greatest in the W matrix, followed by WS, WP, and finally WPS. Losses of particles in the WP and WPS treatment, as compared to the W treatment, seem to have been selective for the larger particles in the distribution, that were similar in size to the PVP-AgNP (Figure 4). The presence of plants resulted in the greatest decrease in Ag in the fractograms. The UV−vis fractograms and associated spectra confirmed the presence of primary particles in all treatments (Figure 4). The peak wavelengths were around 400 nm, which corresponded to the peak wavelength for the original dosing material. The combination of the ICP-MS and DAD fractograms suggested that only primary particles remained within the aqueous phase and losses were primarily due to dissolution as evidenced by increased concentrations in the ultrasupernatants (Figure 2). Losses in the $AgNO_3$ WP and WPS matrices were similar to those in the GA-AgNP treated WP and WPS matrices, supporting the hypothesis that losses were due to binding of ions after dissolution of the GA-AgNPs.

For the $AgNO_3$-treated microcosms, very little Ag appeared in the ICP-MS fractograms for the W and WS treatments, although some Ag was present across the size range of the Ag aggregates observed for W and WS in the PVP-AgNP treatments (Figures S3−S5). It is possible that some of this could have been AgCl particles.[8] Large peaks near the void volume were observed for the WP and WPS samples, and this could have corresponded to DOM-bound Ag (Figure 5, Figure S2). As expected, no UV−vis peaks in the 400−420 nm range were observed in the $AgNO_3$ treatment, reinforcing the conclusion that these peaks corresponded to intact AgNPs in the PVP-AgNP and GA-AgNP treatments (data not shown).

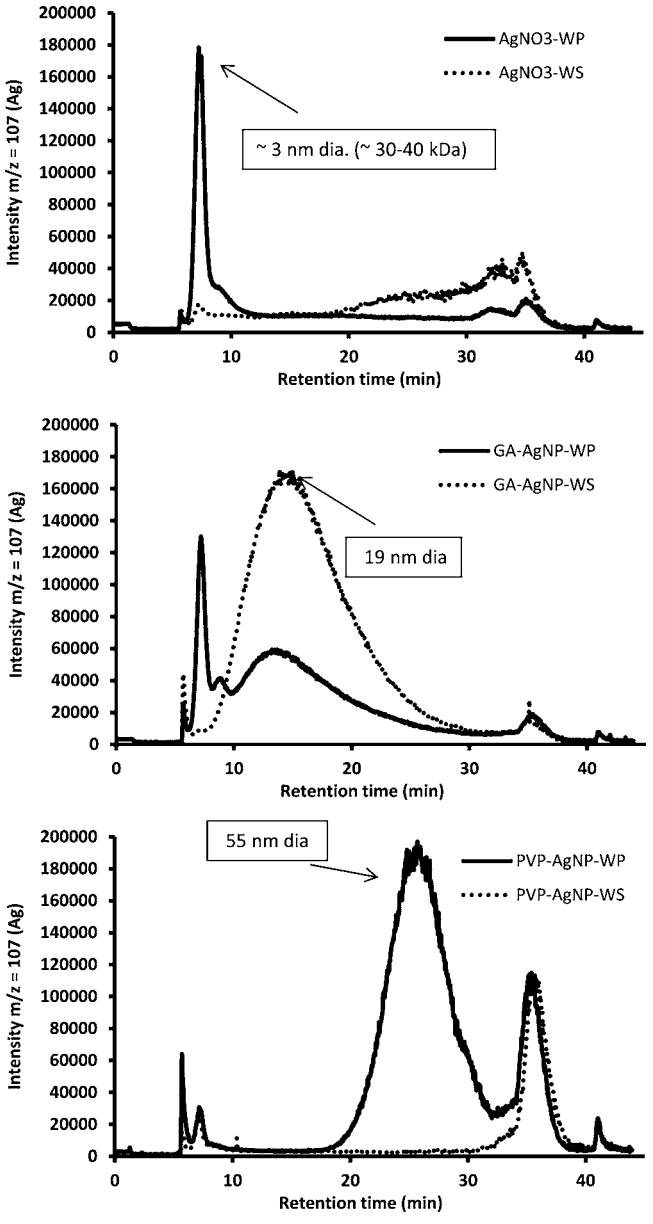

Figure 5. Asymmetrical flow field flow fractograms using ICP-MS detection of Ag control, polyvinylpyrrolidone-coated Ag nanoparticles (PVP-AgNP), gum Arabic-coated Ag nanoparticles (GA-AgNP), and $AgNO_3$-treated microcosms containing water (W), water and sediment (WS), water and plants (WP), or water, plants, and sediment (WPS). Calibrated hydrodynamic diameters are shown below the retention times on the *X* axes. The traces labeled PVP-AgNP and GA-AgNP are for PVP-AgNP and GA-AgNP standards. The starting cross-flow for these fractograms was 2.0 mL min^{-1} decreasing to 0.03 mL min^{-1} in 30 min. The retention time for the void peak is 5.7 min. Calibrated hydrodynamic diameters are indicated for selected peaks in each fractogram.

At high cross-flow, the putative DOM bound fraction of Ag could be baseline resolved from the void peak (Figure 5). A large peak centered at an estimated hydrodynamic diameter of 3 nm, which could correspond to 30−40 kDa organic matter fraction,[18] was observed in every microcosm that contained plants; however, large quantities of Ag were only found in this fraction in the $AgNO_3$ and GA-AgNP treatments, not in the PVP-AgNP treatments. This may explain why there was a much larger difference between the ultrafiltrate and ultrasupernatant Ag concentrations for the GA-AgNP and $AgNO_3$ treatments compared to the PVP-AgNP treatment for most of the matrices. The PVP-AgNP treatment caused less of a DOC increase after 24 h in plant-containing microcosms than the $AgNO_3$ or GA-AgNP treatments.[8] Taken together, this evidence suggests that the presence of aquatic plants may have stimulated the dissolution of GA-AgNPs, as mean ultrasupernatant concentrations were 3−4 times greater in plant-containing treatments than nonplant-containing treatments. Plants had little effect on the PVP-AgNP in terms of dissolution given the similarity of ultrasupernatant concentrations when plants were present or absent.

Validity of the AF4 Separations. Retention times for standard reference materials and light scattering data validated our AF4 separations. In general there was good correspondence between the calculated and observed diameters for the standard reference particles. The sizes measured using DLS or MALLS closely corresponded to the sizes calculated by AF4 theory as well (Figure 6). Recovery of AgNP was consistently near 100% for all treatments except for the water and sediment treatments (Figure S6). The mean recovery for PVP-AgNP in the water and sediment treatments was 50 and 68%, respectively. The losses could not be accounted for by dissolved Ag passing through the 5-kDa MWCO accumulation wall in the instrument because if that were the case, the concentrations in the 3-kDa batch filtrates would have been similar to the amount lost. This indicates that the losses were likely due to particles adhering to the tubing or the channel itself, most likely the accumulation wall. Representative fractograms are shown Figures 3−6. Individual replicates for the ICP-MS fractograms are shown in Figures S3−S5 and S7−S14 to illustrate the variability among replicates. In general there was little variability in the size distributions from replicate microcosms but differing levels of variability in absolute intensity of the fractograms as a whole. Data for Mn, Al, Fe, and Si are not shown because little of these elements was present within the fractograms suggesting heteroaggregates were dominated by organic materials. The samples for individual replicate microcosms were stored for up to 5 months at 4 °C in the dark before AF4 analysis; however, we performed initial analyses on samples composited from all three replicates per mesocosm after only 2 weeks of storage (Figures S15 and S16). The composite samples analyzed after only 2 weeks of storage had similar ICP-MS fractograms as compared to individual replicates analyzed after up to 5 months (Figures S3−S5 and S7−S14). This indicates that the samples changed little during storage.

Effect of Plants on Particle Stability. The microcosms that contained plants had approximately four times the DOC concentrations in GA-AgNP or $AgNO_3$ treatments compared to control microcosms or microcosms containing no plants.[8]

dx.doi.org/10.1021/es204682q | Environ. Sci. Technol. 2012, 46, 6915−6924

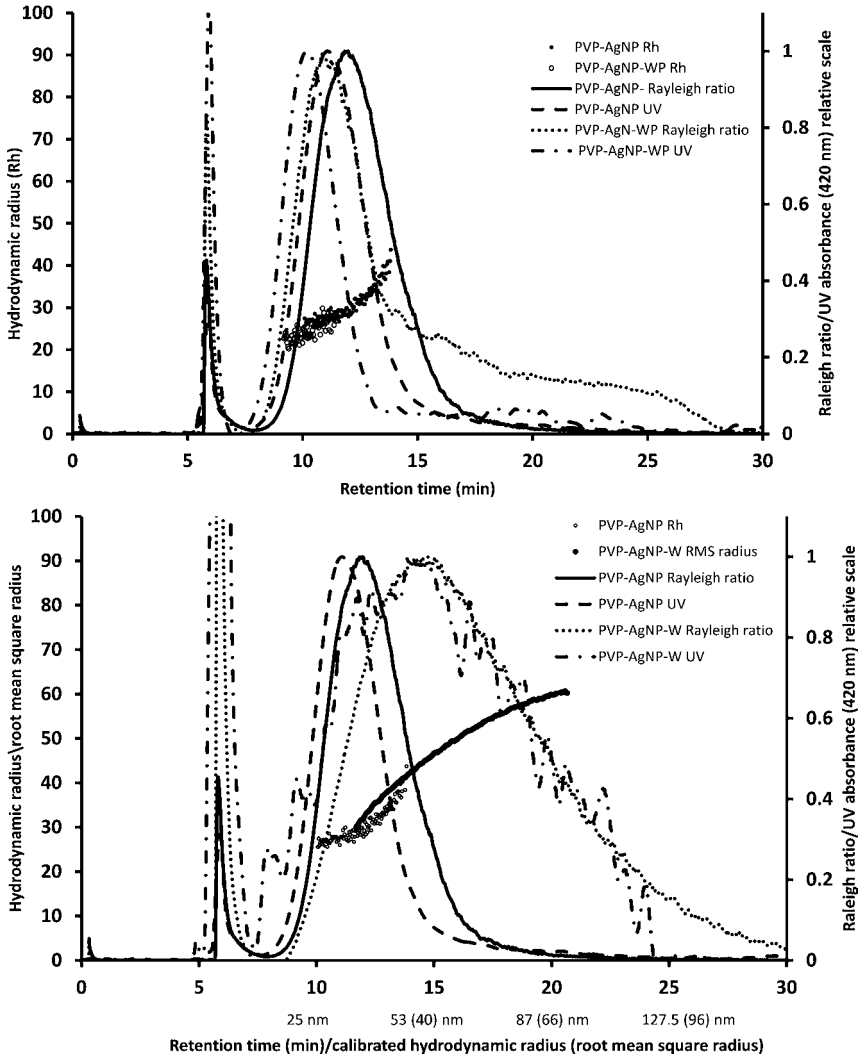

Figure 6. Asymmetrical flow field flow fractograms using ultraviolet−visible (UV−vis) diode array and laser light scattering detection for water samples from polyvinlylpyrrolidone-coated Ag nanoparticles (PVP-AgNPs) microcosms containing water (W) or water and plants (WP). Hydrodynamic radii (Rh) were determined using dynamic light scattering (DLS; top and bottom) or root-mean-square radii (rms) were determined using multiangle laser light scattering (MALLS; bottom) Calibrated Rh values are shown below the retention times on the *X* axes with corresponding rms radii in parentheses. The traces labeled PVP-AgNP are for PVP-AgNP standards. The starting cross-flow was 0.3 mL min^{-1} decreasing to 0.03 mL min^{-1} in 30 min.

PVP-AgNP treated microcosms with plants had smaller increases of DOC versus control, perhaps because they released fewer Ag ions than the GA-AgNP treated microcosms, but the values were still 1.5−2 times greater than those in the control. The presence of the aquatic plants stabilized the PVP-AgNP in the form of primary particles, while in the absence of plants they were extensively aggregated in the form of heteroaggregates. Conversely, the GA-AgNP were seemingly destabilized by the presence of the plants and were removed from the aqueous phase through deposition or dissolution of the particles and subsequent binding of ions to plant or sediment surfaces. Extensive aggregation was not observed in the fractograms and the concentrations in unfiltered and 0.7-μm filtered samples were similar, making aggregation an unlikely explanation for losses of GA-AgNPs. It is tempting to assert that the effects of plant-derived DOM on aggregation and dissolution are due to differences in the particle size distributions rather than the particle coatings; however, this assertion is not supported by the data. The GA-AgNP had a broad particle size distribution that overlapped with the particle size distribution of the PVP-AgNP. If the effects were a result of size, then the GA-AgNP fractograms would have shifted toward longer retention times, since smaller particles would have been preferentially removed, and they did not.

The peak that may have corresponded to DOM in Figure 5 was narrowly distributed with a fwhm of 1.1 min, similar to the peak width of a monodisperse biopolymer, raising the possibility that the substance that increased the DOM concentrations in response to Ag exposure was some form of exudate from one of the plant species that was released in attempt to detoxify the Ag or as a result of Ag toxicity to the plants. We observed a strong fluorescence signal that could be due to the presence of the amino acid tryptophan.[8] This raises the possibility that the exuded or released substance is a protein or contains proteins or peptides. The amount of Ag bound to this substance was similar for both the $AgNO_3$ and GA-AgNP treatments, suggesting that the Ag binding sites may have been saturated given the differing amounts of Ag ions available for binding.

It was shown in the companion study[8] that speciation of the Ag in the particulate phase of the NP-treated matrices (>0.02 μm) determined by L-edge XANES was dominated (>85%) by Ag (0) in the W and WS matrices, indicating relatively minor effects of oxidation or sulfidation on the particles, including oxidation from control additions of KNO_3. In the WP and WPS matrices, the XANES suggested an Ag-cysteine (Ag-Cys) component of the spectra. This component was relatively minor for the PVP-AgNP, but comprised 22−23 and 26−28% of the Ag in the WP and WPS GA treatments, respectively. This indicates that somehow the PVP coating prevented Ag particle oxidation by the plant-derived DOM. The exact mechanism by which the PVP coating prevented oxidation of the PVP-AgNPs by the plant-derived DOM is not clear and further studies are required to uncover it.

Metal binding exudates from multicellular aquatic plants have not been extensively studied. *Egeria densa* was shown to release allelopathic substances that affected the growth of microalgae[19] as well as a metal inducible peptide that is involved in detoxification of Cd.[20] Copper binding proteins have also been identified in the root exudates of a wetland plant *Salicornia europaea*.[21] Much more information is available on metal binding exudates from microalgae. For example, a recent study showed that exudates of *Pseudokirchneriella subcapitata* not only detoxified transition metals, but they also destabilized natural metal binding colloids causing them to aggregate.[22] Another study demonstrated that *P. subcapitata* also produced exudates in response to TiO_2 NP exposure. These exudates may have formed heteroaggregates with the TiO_2 particles helping to decrease water column concentrations.[23]

That AgNPs with different characteristics (particle size distribution and coating) had different effects on release of DOM from plants, and that this DOM in turn had different effects on NP aggregation and dissolution, is a novel finding. This finding highlights how complex interactions between abiotic and biotic components can have significant effects on the fate of engineered nanomaterials, even in a simple model ecosystem. This dynamic interplay between physicochemical properties of nanomaterials and biological responses may have important implications for risks to aquatic communities. Further studies into these interactions investigating more complex systems over longer time periods are needed.

■ ASSOCIATED CONTENT

Supporting Information

Additional information on surface plasmon resonance, recovery for AF4, fractograms for $AgNO_3$ treatments, zeta potential, and variation in fractograms from replicate microcosms. This material is available free of charge via the Internet at http://pubs.acs.org.

■ AUTHOR INFORMATION

Corresponding Author

*E-mail: jason.unrine@uky.edu; phone (859) 257-1657; fax (859) 257-3655; mail: Room N212-N, Agricultural Science Center North, Lexington, KY 40546.

Author Contributions

¶J.M.U. and B.P.C. contributed equally.

Notes

The authors declare no competing financial interest.

■ ACKNOWLEDGMENTS

This material is based upon work supported by the National Science Foundation and the Environmental Protection Agency under NSF Cooperative Agreement EF-0830093, Center for the Environmental Implications of NanoTechnology (CEINT). Additional support was provided by the EPA Science to Achieve Results Program (RD834857) and through cooperative agreement 83515701. Any opinions, findings, conclusions, or recommendations expressed in this material are those of the authors and do not necessarily reflect the views of the NSF or the EPA. A.G. was also supported by the Greek Scholarship Foundation. We gratefully acknowledge P. Bertsch, F. vd Kammer, S. Marinakos, and Y. Cheng.

■ REFERENCES

(1) Luoma, S. *Silver Nanotechnologies and the Environment: Old Problems or New Challenges*; Woodrow Wilson International Center for Scholars, Project on Emerging Nanotechnologies, The Pew Charitable Trusts, PEN-15: 2008.

(2) Fabrega, J.; Luoma, S. N.; Tyler, C. R.; Galloway, T. S.; Lead, J. R. Silver nanoparticles: Behaviour and effects in the aquatic environment. *Environ. Int.* **2011**, *37* (2), 517−531.

(3) Liu, J.; Hurt, R. H. Ion release kinetics and particle persistance in aqueous nano-silver colloids. *Environ. Sci. Technol.* **2010**, *44*, 2169−2175.

(4) Cumberland, S. A.; Lead, J. R. Particle size distributions of silver nanoparticles at environmentally relevant conditions. *J. Chromatogr., A* **2009**, *1216* (52), 9099−9105.

(5) Fabrega, J.; Fawcett, S. R.; Renshaw, J. C.; Lead, J. R. Silver Nanoparticle Impact on Bacterial Growth: Effect of pH, Concentration, and Organic Matter. *Environ. Sci. Technol.* **2009**, *43*, 7285−7290.

(6) Kennedy, A. J.; Hull, M. S.; Bednar, A. J.; Goss, J. D.; Gunter, J. C.; Bouldin, J. L.; Vikesland, P. J.; Steevens, J. A. Fractionating Nanosilver: Importance for Determining Toxicity to Aquatic Test Organisms. *Environ. Sci. Technol.* **2010**, *44* (24), 9571−9577.

(7) Shoults-Wilson, W. A.; Reinsch, B. C.; Tsyusko, O. V.; Bertsch, P. M.; Lowry, G. V.; Unrine, J. M. Role of Particle Size and Soil Type in Toxicity of Silver Nanoparticles to Earthworms. *Soil Sci. Soc. Am. J.* **2011**, *75* (2), 365−377.

(8) Bone, A.; Colman, B.; Gondikas, A.; Newton, K.; Harrold, K.; Unrine, J.; Klaine, S.; Matson, C.; DiGiulio, R. Complex environmental media in aquatic microcosms determines the behavior and toxicity of silver nanoparticles, Part 2: Toxicity and Ag speciation. *Environ. Sci. Technol.* **2012**, DOI: DOI:10.1021/es204683m.

(9) Poda, A. R.; Bednar, A. J.; Kennedy, A. J.; Harmon, A.; Hull, M.; Mitrano, D. M.; Ranville, J. F.; Steevens, J. Characterization of silver nanoparticles using flow-field flow fractionation interfaced to inductively coupled plasma mass spectrometry. *J. Chromatogr., A* **2011**, *1218* (27), 4219−4225.

(10) Kim, S. T.; Kang, D. Y.; Lee, S.; Kim, W.-S.; Lee, J. T.; Cho, H. S.; Kim, S. H. Separation and quantitation of silver nanoparticles using sedimentation field-flow fractionation. *J. Liq. Chromatogr. Relat. Technol.* **2007**, *30* (17), 2533−2544.

(11) Liu, F. K.; Wei, G. T. Effect of mobile-phase additives on separation of gold nanoparticles by size-exclusion chromatography. *Chromatographia* **2004**, *59* (1−2), 115−119.

(12) Plathe, K. L.; von der Kammer, F.; Hassellov, M.; Moore, J.; Murayama, M.; Hofmann, T.; Hochella, M. F., Jr. Using FlFFF and aTEM to determine trace metal-nanoparticle associations in riverbed sediment. *Environ. Chem.* **2010**, *7* (1), 82−93.

(13) Kelley, M. Distribution and biomass of aquatic macrophytes in an abandoned nuclear cooling resevoir. *Aquat. Bot.* **1989**, *35*, 133−152.

(14) Cheng, Y.; Yin, L.; Lin, S.; Wiesner, M.; Bernhardt, E.; Liu, J. Toxicity Reduction of Polymer-Stabilized Silver Nanoparticles by Sunlight. *J. Phys. Chem. C* **2011**, *115* (11), 4425−4432.

(15) Wahlund, K. G.; Giddings, J. C. Properties of an Asymmetrical Flow Field-Flow Fractionation Channel Having One Permeable Wall. *Anal. Chem.* **1987**, *59* (9), 1332−1339.
(16) Moon, J.; Kim, S. H.; Cho, J. Characterizations of natural organic matter as nano particle using flow field-flow fractionation. *Colloids Surf., A* **2006**, *287* (1−3), 232−236.
(17) Ei-Sayed, M. A.; Link, S. Optical properties and ultrafast dynamics of metallic nanocrystals. *Annu. Rev. Phys. Chem.* **2003**, *54*, 331−366.
(18) Assemi, S.; Newcombe, G.; Hepplewhite, C.; Beckett, R. Characterization of natural organic matter fractions separated by ultrafiltration using flow field-flow fractionation. *Water Res.* **2004**, *38* (6), 1467−1476.
(19) Vanderstukken, M.; Mazzeo, N.; Van Colen, W.; Declerck, S. A. J.; Muylaert, K. Biological control of phytoplankton by the subtropical submerged macrophytes *Egeria densa* and *Potamogeton illinoensis*: A mesocosm study. *Freshwater Biol.* **2011**, *56* (9), 1837−1849.
(20) Aravind, P.; Prasad, M. N. V. Zinc protects chloroplasts and associated photochemical functions in cadmium exposed *Ceratophyllum demersum* L., a freshwater macrophyte. *Plant Sci.* **2004**, *166* (5), 1321−1327.
(21) Pan, X.; Yang, J.; Zhang, D.; Chen, X.; Mu, S. Cu(II) complexation of high molecular weight (HMW) fluorescent substances in root exudates from a wetland halophyte (*Salicornia europaea* L.). *J Biosci. Bioeng.* **2011**, *111* (2), 193−197.
(22) Koukal, B.; Rosse, P.; Reinhardt, A.; Ferrari, B.; Wilkinson, K. J.; Loizeau, J.-L.; Dominik, J. Effect of *Pseudokirchneriella subcapitata* (Chlorophyceae) exudates on metal toxicity and colloid aggregation. *Water Res.* **2007**, *41* (1), 63−70.
(23) Hartmann, N. B.; Von der Kammer, F.; Hofmann, T.; Baalousha, M.; Ottofuelling, S.; Baun, A. Algal testing of titanium dioxide nanoparticles-Testing considerations, inhibitory effects and modification of cadmium bioavailability. *Toxicology* **2010**, *269* (2−3), 190−197.